iScience

CellPress
OPEN ACCESS

Article

Plasmodium falciparum infection reshapes the human microRNA profiles of red blood cells and their extracellular vesicles

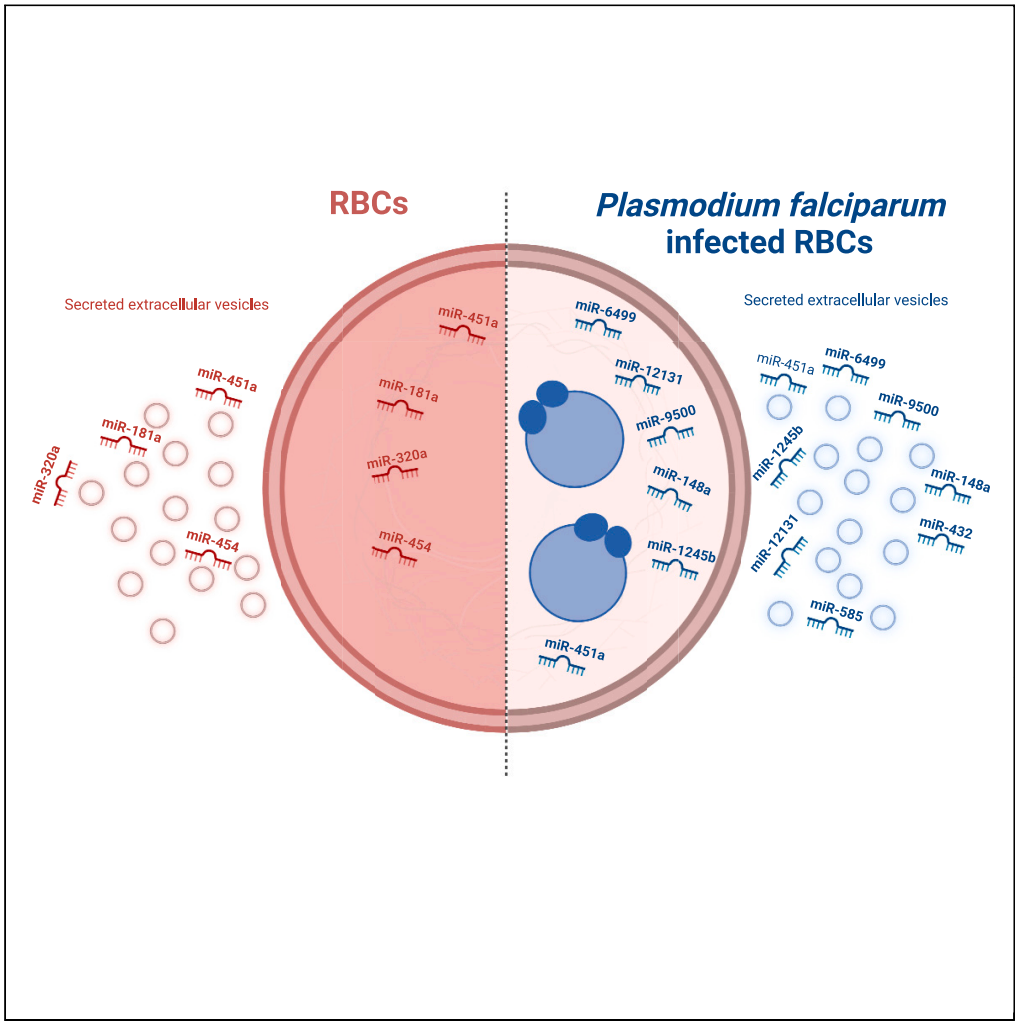

Yifan Wu, Stephanie Leyk, Hanifeh Torabi, ..., Thomas Jacobs, Iris Bruchhaus, Nahla Galal Metwally

metwally@bnitm.de

Highlights

Nine miRNAs were highly expressed in red blood cells after *P. falciparum* infection

Members of the let-7 family were downregulated in red blood cells after infection

Hsa-miR-451a was the most abundant secreted miRNA within RBCs

The identified miRNAs target genes that play roles in immune responses

Wu et al., iScience 26, 107119
July 21, 2023 © 2023 The Author(s).
https://doi.org/10.1016/j.isci.2023.107119

iScience

CellPress
OPEN ACCESS

Article

Plasmodium falciparum infection reshapes the human microRNA profiles of red blood cells and their extracellular vesicles

Yifan Wu,[1] Stephanie Leyk,[2] Hanifeh Torabi,[1] Katharina Höhn,[3] Barbara Honecker,[1] Maria del Pilar Martinez Tauler,[1] Dániel Cadar,[4] Thomas Jacobs,[2] Iris Bruchhaus,[1,5] and Nahla Galal Metwally[1,6,*]

SUMMARY

***Plasmodium falciparum*, a human malaria parasite, develops in red blood cells (RBCs), which represent approximately 70% of all human blood cells. Additionally, RBC-derived extracellular vesicles (RBC-EVs) represent 7.3% of the total EV population. The roles of microRNAs (miRNAs) in the consequences of *P. falciparum* infection are unclear. Here, we analyzed the miRNA profiles of non-infected human RBCs (niRBCs), ring-infected RBCs (riRBCs), and trophozoite-infected RBCs (trRBCs), as well as those of EVs secreted from these cells. Hsa-miR-451a was the most abundant miRNA in all RBC and RBC-EV populations, but its expression level was not affected by *P. falciparum* infection. Overall, the miRNA profiles of RBCs and their EVs were altered significantly after infection. Most of the differentially expressed miRNAs were shared between RBCs and their EVs. A target prediction analysis of the miRNAs revealed the possible identity of the genes targeted by these miRNAs (CXCL10, OAS1, IL7, and CCL5) involved in immunomodulation.**

INTRODUCTION

Malaria has a major impact on human health worldwide. According to the World Health Organization, malaria killed 627,000 people in 2020, representing a 12% increase in the death rate from 2019, which was attributed to service disruption due to the COVID-19 pandemic. Notably, 77% of the malaria-related deaths in 2020 were children under 5 years of age.[1] In the same year, 11.6 million pregnant women were diagnosed with malaria infection, resulting in 819,000 children with low birth weight.[1] Malaria is caused by five species of the genus *Plasmodium*, although *P. falciparum* is responsible for most malaria-related deaths.[1]

Cerebral malaria (CM) is a severe neurological complication of *P. falciparum* infection. The pathogenic basis of CM is poorly understood, but cytoadhesion and the host immune response are thought to be involved. Red blood cells (RBCs) have long been recognized as a perfect shelter for *Plasmodium* parasitic invaders, providing them with not only abundant food resources but also protection against host immune attacks. Upon entry into RBCs, *P. falciparum* uses different strategies to survive. For example, the parasite changes the morphology of infected RBCs (iRBCs) by inducing the production of knob-like protrusions on the cell surface.[2] These protrusions provide a scaffold for the correct presentation of the parasite's major virulence protein, erythrocyte membrane protein 1 (*Pf*EMP1), thereby stabilizing the binding of iRBCs to human endothelial cell (EC) receptors.[3,4]

The main function of terminally differentiated RBCs is oxygen transportation via hemoglobin. During differentiation to their mature form, RBCs gradually lose cellular organelles and a lot of their nucleic acid content (the long-held belief that mature RBCs lack DNA and RNA is now recognized to be wrong). RNA sequencing (RNA-seq) technologies have revealed that mature RBCs contain some mRNAs and microRNAs (miRNAs).[5–8] Indeed, recent estimates have suggested that RBCs express approximately 8,092 mRNAs and 359 miRNAs.[9,10] Many of the most highly expressed RBC-mRNAs encode proteins that are associated with erythroid differentiation. In addition, RBCs express mRNAs that encode proteins involved in the initiation, activation, and regulation of transcription and translation (such as RNA polymerases I, II, and III; zinc/ plant homeodomain (PHD) finger DNA-binding proteins; and cysteinyl- and lysyl-tRNA synthetases), as well as

[1]Research Group Host Parasite Interaction, Bernhard Nocht Institute for Tropical Medicine, Hamburg, Germany

[2]Research Group Protozoa Immunology, Bernhard Nocht Institute for Tropical Medicine, Hamburg, Germany

[3]Cellular Parasitology Department, Bernhard Nocht Institute for Tropical Medicine, Hamburg, Germany

[4]Arbovirology Department, Bernhard Nocht Institute for Tropical Medicine, Hamburg, Germany

[5]Biology Department University of Hamburg, Hamburg, Germany

[6]Lead contact

*Correspondence: metwally@bnitm.de

https://doi.org/10.1016/j.isci.2023.107119

This is an open access article under the CC BY-NC-ND license (http://creativecommons.org/licenses/by-nc-nd/4.0/).

important RNA-stabilizing factors (such as poly(A)-binding proteins and the antiapoptotic proteins beclin 1, reticulon 4, B-cell lymphoma 2 [BCL2], and inhibitor of apoptosis [IAP]).[11]

miRNAs are small noncoding RNAs that inhibit the expression of approximately 60% of protein-coding genes. Direct interaction of miRNAs through complementary base pairing leads to cleavage of their target mRNAs.[12] In addition, a high concentration of miRNAs causes hypermethylation of genes encoding target mRNAs, resulting in downregulation of gene transcription.[13] Under normal physiological conditions, miRNAs have unique expression profiles within each organ. Pathogen invasion of host cells causes dysregulation of miRNA profiles.[14,15] Some pathogens preferentially invade certain tissues, leading to tissue-specific alterations in miRNA profiles[16] that can either lead to host protection or increase the pathogenic effect of the invading organism.[17,18]

RBC-miRNAs play a key role in hematopoiesis and the maturation of RBCs[6,19–22] and are also involved in the development of specific diseases such as atherosclerosis.[23] Six abundant RBC-miRNAs have been identified to date, namely, miR-451a, miR-144-3p, miR-16, miR-92a, let-7, and miR-486-5p.[10] RBCs of the sickle cell phenotype are also enriched with specific miRNAs that lead to growth inhibition of the malaria parasite through the translational repression of parasite mRNAs.[8] Chakrabarti and colleagues also reported that human miR-197-5p inhibits the *P. falciparum* apicortin which affects the parasite growth.[24] Adding to this, other researchers postulated that after RBCs invasion the human RNA-induced silencing complex (RISC) complex is imported into the parasite which might interact with the *Plasmodium* mRNA and regulate their stability and translation.[25]

Currently, minimal information is available on the role of miRNAs in the pathogenesis of *P. falciparum* complications. In addition, to our knowledge, a comprehensive analysis of the human RBC-miRNA profile has not yet been performed.

Viable cells communicate indirectly by releasing extracellular vesicles (EVs) that contain miRNAs, mRNAs, and proteins. EVs are either formed inside multivesicular bodies (exosomes) or directly from the plasma membrane (microvesicles). EVs released from RBCs contain miRNAs coupled with Argonaute 2; these complexes can alter gene expression in other types of cells upon uptake of the RBC-EVs.[26–31]

Here, to identify the potential roles played by miRNAs during *P. falciparum* infection, we examined the expression levels of RBC-miRNAs, RBC-EV-miRNAs, and RBC-mRNAs in both non-infected RBCs (niRBCs) and *P. falciparum* iRBCs. Further investigations in this area could inspire the development of novel miRNAs-based therapeutics.

RESULTS

Isolation of RBC-miRNAs, RBC-EV-miRNAs, and RBC-mRNAs

An overview of the procedure used to isolate and characterize RBC-miRNAs, RBC-EV-miRNAs, and RBC-mRNAs is shown in (Figure 1A). niRBCs and *P. falciparum* iRBCs were cultivated as described previously.[32] The *P. falciparum* culture was tightly synchronized to enrich stage-specific iRBCs for the isolation of miRNA, mRNA, and EVs (ring-stage iRBCs [riRBCs] or trophozoite-stage iRBCs [trRBCs]).[33] RBC-miRNAs and RBC-mRNAs were isolated from cells as controls. RBC-EVs were also purified from the culture supernatants of niRBCs, riRBCs, and trRBCs, as described previously.[28] Subsequently, RBC-EV-miRNAs were isolated. The RBC-miRNAs, RBC-EV-miRNAs, and RBC-mRNAs were subjected to next-generation sequencing (NGS), and the obtained sequences were aligned to the human miRNA/transcriptome reference sequences.

Transmission electron microscopy following incubation with an antibody targeting cluster of differentiation 235a (CD235a), a membrane-bound sialoglycoprotein present on mature RBCs, confirmed that the isolated EVs did indeed originate from the niRBCs, riRBCs, and trRBCs (Figure 1B). This analysis also confirmed that the purified EVs displayed the expected circular morphology,[34,35] with an average size of approximately 150–200 nm. In addition, a nanoparticle tracking assay confirmed that the average size of all three EV populations was 100–250 nm (Figure 1C).

Identification of abundant miRNAs in RBCs

A previous study using NGS identified 287 known and 72 putative novel RBC-miRNAs.[10] A later study found that several miRNAs, including miR-451, miR-486-5p, and miR-144-3p, are expressed at high levels in RBCs.[36]

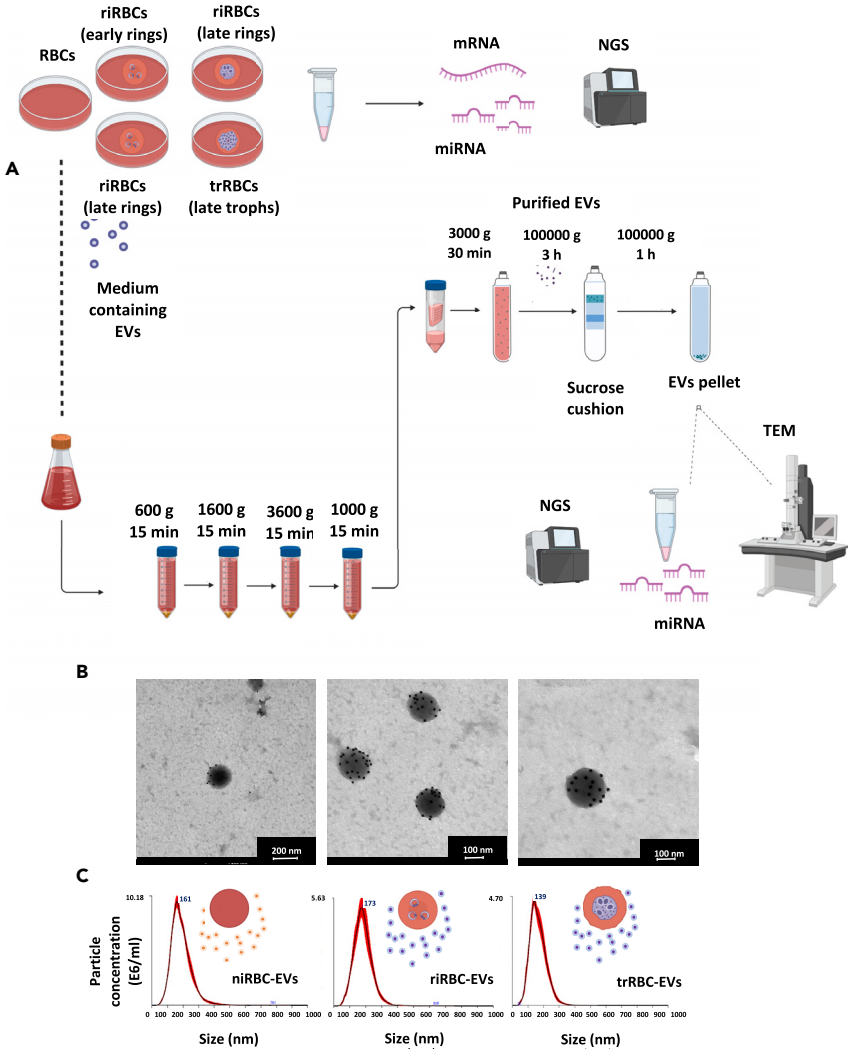

Figure 1. Schematic overview of the workflow used to isolate and characterize RBC-miRNAs

(A) RBC-EV-miRNAs, and RBC-mRNAs. RBCs infected with *P. falciparum* and their culture supernatants (containing EVs) were harvested as riRBCs and trRBCs. As a control, niRBCs were cultured in the same medium and the supernatant was also harvested. The culture supernatants were centrifuged sequentially to isolate EVs. RBC-mRNAs and RBC-miRNAs were purified from the cultivated RBCs. Finally, RBC-EV-miRNAs were purified from the isolated EVs.

(B) Transmission electron microscopy was performed to confirm the presence of EVs after purification. niRBCs, riRBCs, and trRBCs were incubated with an antibody targeting human CD235a and then subjected to immunogold labeling.

(C) The left, middle, and right graphs show nanoparticle tracking analyses of EVs from niRBCs, riRBCs, and trRBCs, respectively.

Here, we found that miR-451a was the most abundant miRNA in niRBCs, riRBCs, and trRBCs but was expressed at a similar level in all three cell types, with average normalized expression levels of 17×10^6, 16.7×10^6, and 15.7×10^6, respectively. Similarly, miR-451a was abundant in the EVs isolated from niRBCs, riRBCs, and trRBCs, but its expression level did not differ significantly between the three EV populations, with average normalized expression levels of approximately 8.6×10^5, 6.5×10^5, and 6.8×10^5, respectively (Figure 2).

Differential expression of miRNAs in iRBCs versus niRBCs

Next, we used C-C motive chemokine ligand 2 (CLC) Genomics software V22 to identify miRNAs that were differentially expressed in riRBCs or trRBCs versus niRBCs. Clean NGS reads were aligned to the miRbase v22 database. Overall, the expression levels of 206 and 26 miRNAs were significantly upregulated and downregulated (fold change >5), respectively, in riRBCs versus niRBCs (Figure 3A). Furthermore, 321 and 53 miRNAs were significantly upregulated and downregulated (fold change >5),

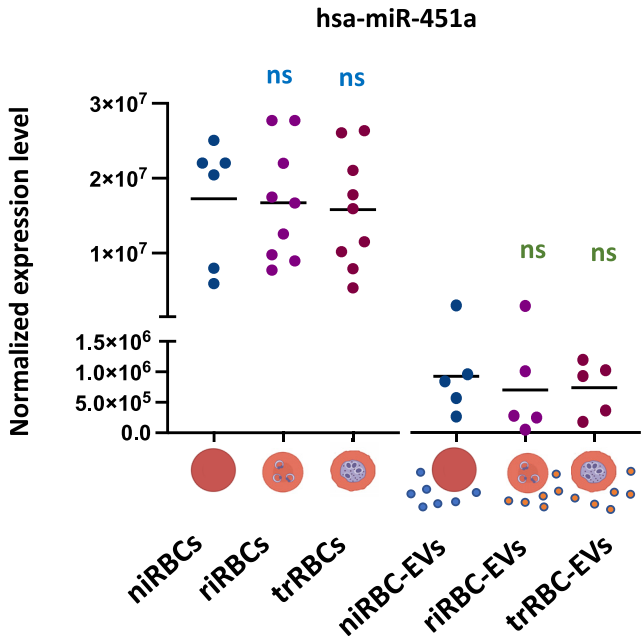

Figure 2. Expression of hsa-miR-451a in niRBCs, riRBCs, and trRBCs, as well as in EVs isolated from these cell types

The comparisons were performed using the differential expression function in the CLC Genomics software V22. Statistical significance was calculated based on an FDR-adjusted p value <0.05 (ns = nonsignificant) (FDR = False Discovery Rate).

respectively, in trRBCs versus niRBCs (Figure 3B). Figure 3C shows a heatmap of the top 50 miRNAs that were highly expressed in both riRBCs and trRBCs versus niRBCs (see also Table S1). To generate the heatmap, we used the normalized expression values (total counts) from the differential expression function in CLC Genomics software V22, and statistical significance was calculated using a 10% false discovery rate (FDR)-adjusted p value. The heatmap showed very low, homogeneous expression of these 50 miRNAs in niRBCs (RBCs 1–6 in Figure 3E). However, a marked color change in the heatmap was evident for the infected populations (Rings 1–9 and Trophs 1–9 in Figure 3C), indicating increased expression of the miRNAs. In general, expression of the 50 miRNAs was increased slightly in the riRBCs harvested at 4–6 h postinvasion (Rings 1–3 in Figure 3C) but was increased more prominently in the riRBCs harvested at 8–14 h postinvasion (Rings 4–9 in Figure 3C). The raw reads were deposited in NCBI (Bioproject Number: PRJNA897869).

Differential expression of miRNAs in iRBC-EVs versus niRBC-EVs

A comparison of the distribution of miRNAs in the isolated EVs revealed that 63 and 53 miRNAs were significantly upregulated and downregulated, respectively, in riRBC-EVs versus niRBC-EVs (Figure 3D). Furthermore, 144 and 72 miRNAs were significantly upregulated and downregulated (fold change >5), respectively, in trRBC-EVs versus niRBC-EVs (Figure 3E). Figure 3F shows a heatmap of the top 12 miRNAs that were differentially expressed in both riRBC-EVs and trRBC-EVs versus niRBC-EVs (see also Table S2). The heatmap was generated as described in the earlier section. As seen for the differentially expressed miRNAs in the RBCs, the majority of the top 12 miRNAs that were differentially expressed in the isolated EVs showed very low, homogeneous expression in EVs from uninfected cells (RBCs 1–5 in Figure 3F), with increased expression in the infected populations (Rings 1–5 and Trophs 1–5 in Figure 3F).

Identification of common differentially expressed miRNAs in riRBCs and riRBC-EVs versus uninfected controls

Overall, the expression levels of 393 miRNAs were upregulated significantly in riRBCs versus niRBCs, and those of 63 miRNAs were upregulated significantly in riRBC-EVs versus niRBC-EVs (fold change cutoff ≥ 2). An analysis of the common upregulated miRNAs revealed that 30 were highly differentially expressed in both riRBCs and riRBC-EVs (Figure 3G). The subsections in the following focus on the top nine common

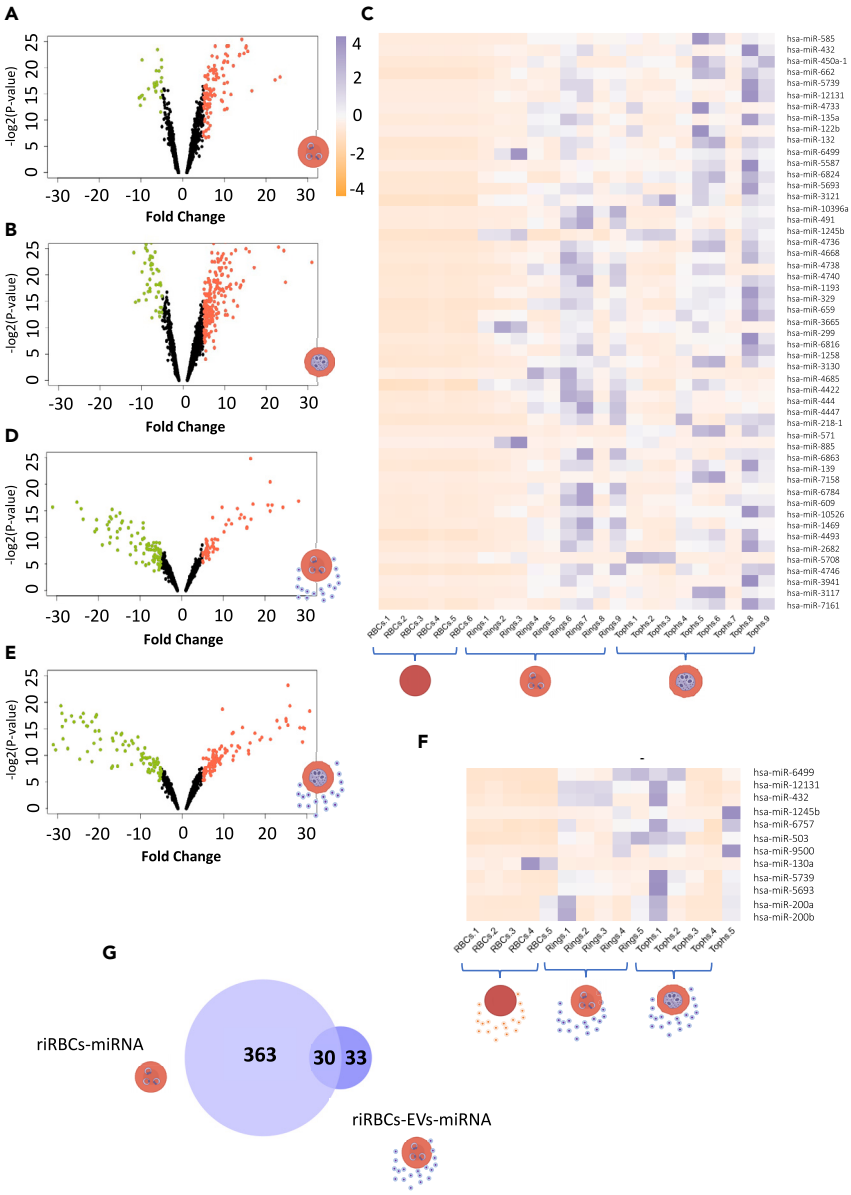

Figure 3. miRNA profiles among iRBCs and EVs

(A–E) Volcano plots showing the distributions of the normalized expression levels of miRNAs in riRBCs versus niRBCs (A), trRBCs versus niRBCs (B), riRBC-EVs versus niRBCs-EVs (D), and trRBC-EVs versus niRBCs-EVs (E). The volcano plots were generated using the R program (for the script, please see STAR Methods). (C and F) Heatmaps representing the expression levels of the top 50 miRNAs that were differentially expressed in both riRBCs and trRBCs versus niRBCs (C) and the top 12 miRNAs that were significantly highly expressed in both riRBCs-EVs and trRBCs-EVs versus niRBCs-EVs (F). The heatmaps were produced using the pheatmap R package[37] (for the script, please see STAR Methods).

(G) A Venn diagram showing the overlap between the numbers of miRNAs that were differentially expressed in riRBCs versus niRBCs and in riRBC-EVs versus niRBC-EVs. The miRNAs included in the comparison were highly expressed, with a fold change of at least 2 versus the uninfected control and FDR p value <0.05.

upregulated miRNAs (those with the highest statistical significance) and their target genes identified by Ingenuity Pathway Analysis (IPA) software. The top nine miRNA candidates are listed in Table 1.

hsa-miR-6499-3p (Figure 4A). The *NFKBIA* gene was predicted as a target of miR-6499-3p. NFKBIA is involved in acute phase response signaling, including the activation of neutrophils and T cells (Tables S3

Table 1. Top highly expressed miRNA candidates in both iRBCs and iRBCs-EVs

miRNA	Accession number	Sequence	Target gene (Predicted)
hsa-miR-6499-3p	MIMAT0025451	AGCAGUGUUUGUUUUGCCCACA	*NFKBIA*
hsa-miR-432-5p	MIMAT0025450	UCGGGCGCAAGAGCACUGCAGU	IL7
hsa-miR-585-5p	MIMAT0026618	CUAGCACACAGAUACGCCCAGA	*IL6ST*
hsa-miR-12131	MI0039733	UCCCUGCCCUUUAUUUGGGAGUACACCUC UCCAAAUAUACAGUUAACUGAUGUUUUAC UGUUUAUUUGGAGAGGUGUACUCCCAAA UAAAGGGCAUACCCUC	-
hsa-miR-1245b-5p	MI0017431	UUUAUAUGUAGGCCUUUAGAUCACU UAAAGAGUAUUCAACAUCAG AUGAUCUAAAGGCCUAUACAUAAA	MAPK13
hsa-miR-662	MI0003670	GCUGUUGAGGCUGCGCAGCCAGGCCCU GACGGUGGGGUGGCUGCGGGCCUUCU GAAGGUCUCCCACGUUGUGGCCCAGCAG CGCAGUCACGUUGC	LTBR
hsa-miR-148a-5p	MI0000253	GAGGCAAAGUUCUGAGACACUCCGACU CUGAGUAUGAUAGAAGUCAGUGCACU ACAGAACUUUGUCUC	*IL22*
hsa-miR-9500	MI0029185	AAAAGGGAAGAUGGUGACCACAUAGG AGGGACAGCGGCCUUUCCAACAGGGG ACCCUUGCCAGCC	CXCL10
hsa-miR-12136	MI0039740	GAAAAAGUCAUGGAGGCCAUGGGGUU GGCUUGAAACCAGCUUUGGGGG GUUCGAUUCCUUCCUUUUUUGUC	-

*Relative KD: values are predicted using a convolutional neural network (CNN) that predicts binding affinity between miRNA and any 12-nt sequence (Targetscan V8 Human).

and S4). The gene encoding ULBP3, which is involved in natural killer cell signaling, was also predicted as a target (Figures 5A and 5B) (Tables S3 and S4).

hsa-miR-432-5p (Figure 4B). Among others, the gene encoding interlukin-7 (IL7), which is involved in both the IL7 and JAK1/JAK2 cytokine signaling pathways, was predicted as a target of miR-432-5p (Figures 5A and 5B) (Tables S3 and S4).

hsa-miR-585-5p (Figure 4C). The interlukin-6 (*IL6ST)* gene was predicted as a target of miR-585-5p. *IL6ST* is involved in the acute phase signaling pathway as well as IL6 cytokine signaling (Figures 5A and 5B) (Tables S3 and S4).

hsa-miR-12131 (Figure 4D). No targets were predicted for this miRNA.

hsa-miR-1245b-5p (Figure 4E). The gene encoding MAPK13, which plays a role in T lymphocyte and acute phase signaling, was predicted as a target of miR-1245b-5p (Figures 5A and 5B) (Tables S3 and S4).

hsa-miR-662 (Figure 4F). The gene encoding LTBR, which is involved in intercellular crosstalk between dendritic cells and natural killer cells, was predicted as a target of miR-662 (Figures 5A and 5B) (Tables S3 and S4). **hsa-miR-148a-5p** (Figure 4G). Among others, miR-148a-5p is predicted to target the gene encoding OAS1, which plays a role in interferon signaling. The interlukin-22 (*IL22*) gene was also identified as a target of miR-148a-5p (Figures 5A and 5B) (Tables S3 and S4).

hsa-miR-9500 (Figure 4H). Among others, miR-9500 is predicted to target the gene encoding C-X-C motif chemokine ligand 10 (CXCL10), which mediates communication between the innate and adaptive immune systems (Figures 5A and 5B) (Tables S3 and S4).

hsa-miR-12136 (Figure 4I). No targets were predicted for this miRNA.

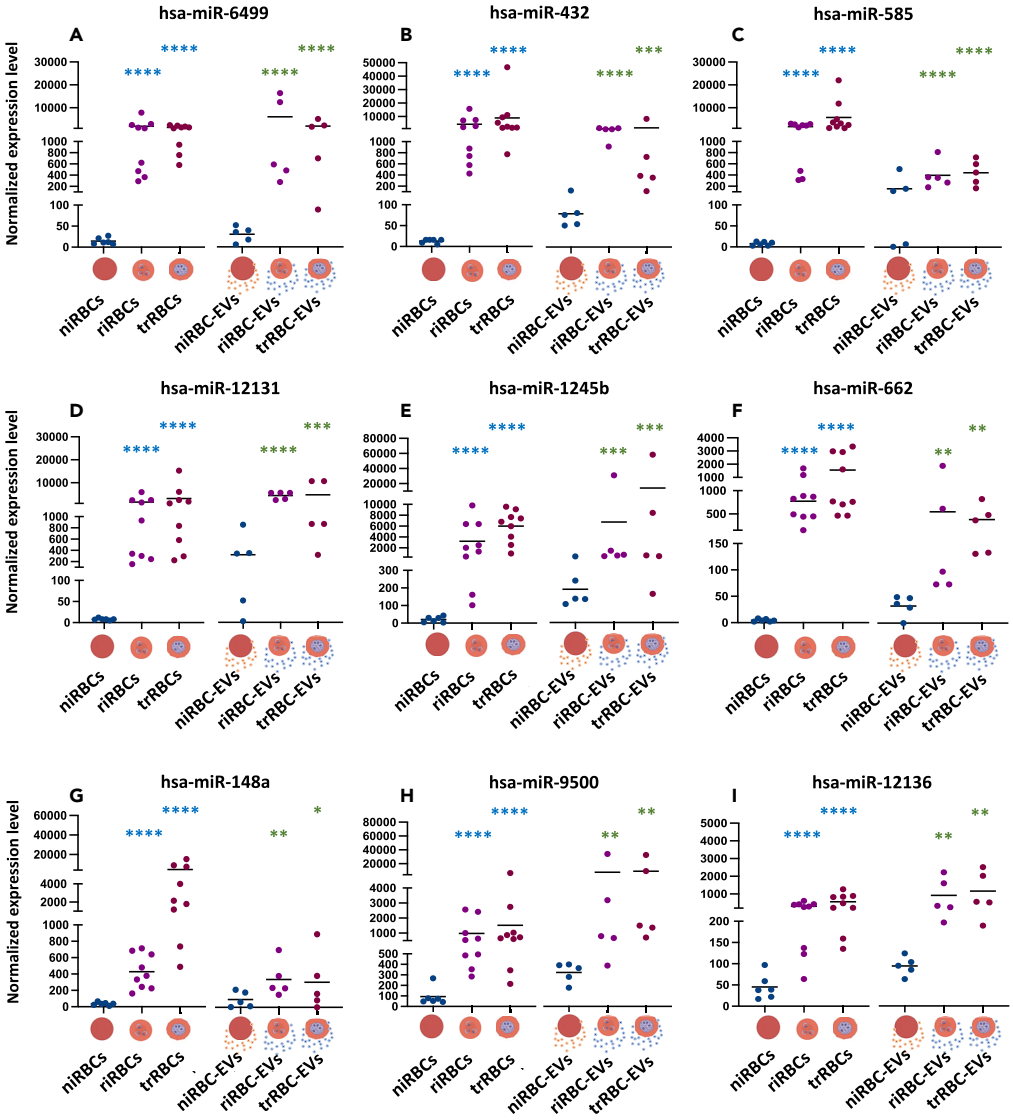

Figure 4. The expression levels of the top significantly highly expressed miRNAs in riRBCs and trRBCs versus niRBCs and in riRBC-EVs and trRBC-EVs versus niRBC-EVs

(A–I) (A) hsa-miR-6499, (B) hsa-miR-432, (C) hsa-miR-585, (D) hsa-miR-12131, (E) hsa-miR-1245b, (F) hsa-miR-662, (G) hsa-miR-148a, (H) hsa-miR-9500 and (I) hsa-miR-12136. The comparisons were performed using the differential expression function in CLC Genomics software V22. Statistical significance was calculated based on an FDR-adjusted p value (*$p < 0.05$, **$p < 0.01$, ***$p < 0.001$ and ****$p < 0.0001$).

Functional analysis of highly expressed miRNA candidates

IPA software was used to identify the target genes for the aforementioned miRNA candidates. Table S4 lists the target genes and their functions. Search Tool for the Retrieval of Interacting Genes/Proteins (STRING) database was used to cluster the target genes. The K-means clustering method was used to allocate the proteins encoded by these genes into four main clusters according to the experimental records within different databases (Figure 5A). The blue cluster includes 19 nodes corresponding to genes related to immune-regulatory interactions. The red cluster consists of 23 nodes corresponding to genes related to plasma membrane and cell signaling. The yellow cluster contains 23 nodes corresponding to genes related to hypoxia-inducible factor 1 (HIF-1) and phagosome pathways. Finally, the green cluster contains 18 nodes corresponding to genes encoding proteins involved in cytokine receptor activity and T cell chemotaxis (for example: IL7, CXCL10, CCL5, and tumor necrosis factor super family 4 [TNFSF4]) (Figures 5A and 5B).

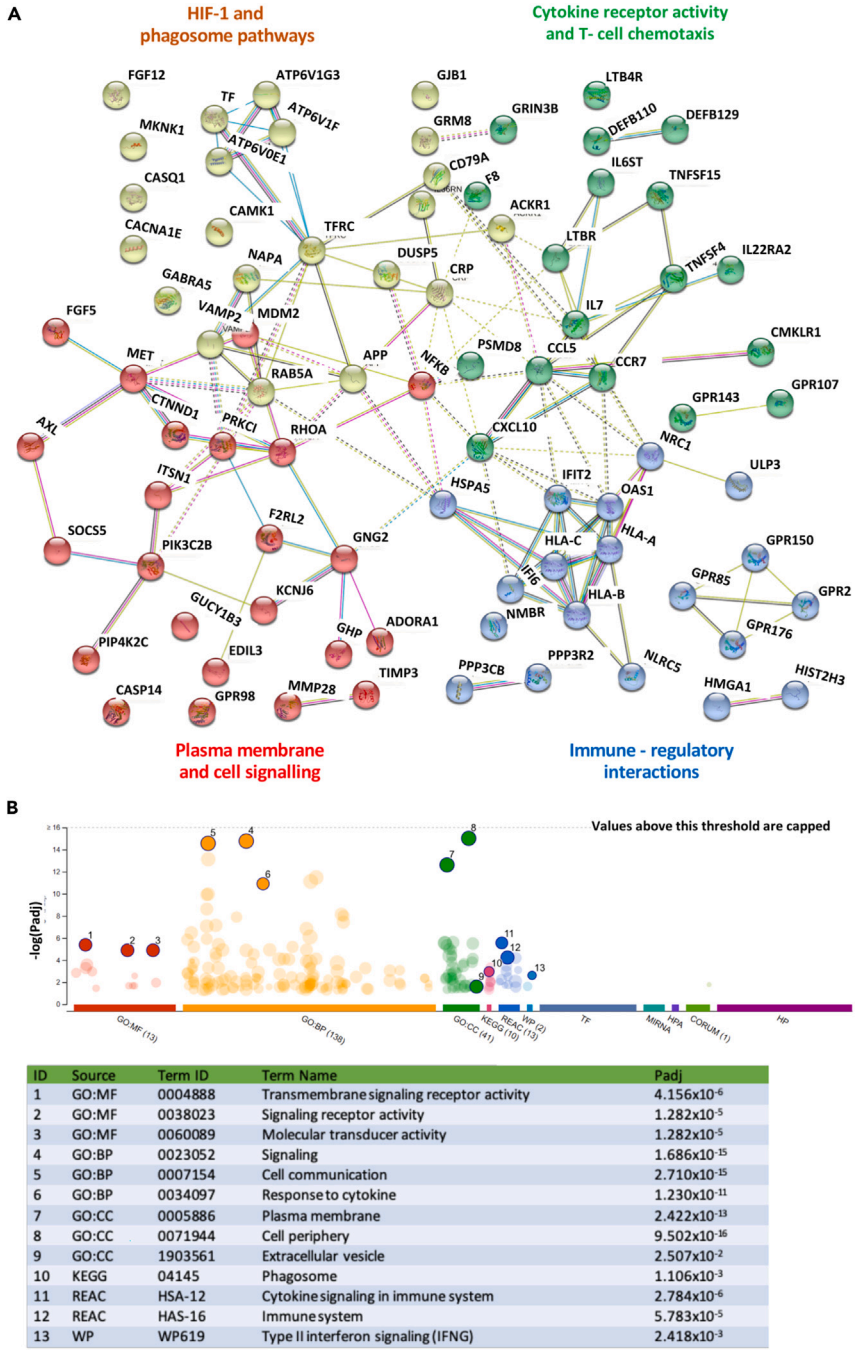

ID	Source	Term ID	Term Name	Padj
1	GO:MF	0004888	Transmembrane signaling receptor activity	4.156×10^{-6}
2	GO:MF	0038023	Signaling receptor activity	1.282×10^{-5}
3	GO:MF	0060089	Molecular transducer activity	1.282×10^{-5}
4	GO:BP	0023052	Signaling	1.686×10^{-15}
5	GO:BP	0007154	Cell communication	2.710×10^{-15}
6	GO:BP	0034097	Response to cytokine	1.230×10^{-11}
7	GO:CC	0005886	Plasma membrane	2.422×10^{-13}
8	GO:CC	0071944	Cell periphery	9.502×10^{-16}
9	GO:CC	1903561	Extracellular vesicle	2.507×10^{-2}
10	KEGG	04145	Phagosome	1.106×10^{-3}
11	REAC	HSA-12	Cytokine signaling in immune system	2.784×10^{-6}
12	REAC	HAS-16	Immune system	5.783×10^{-5}
13	WP	WP619	Type II interferon signaling (IFNG)	2.418×10^{-3}

Figure 5. Functional analysis of the miRNA candidates

(A) STRING clustering of the predicted target genes of the top differentially expressed miRNAs shown in Figure 4. Four clusters were identified using K-means clustering: blue cluster (immune-regulatory interactions), red cluster (plasma membrane and cell signaling), yellow cluster (HIF-1 and phagosome pathways), and green cluster (cytokine receptor activity and T cell chemotaxis). The blue and pink connector lines represent the database and experimentally confirmed interactions, respectively.

(B) A g:Profiler graph showing the significant biological pathways affected by the predicted target genes. Transmembrane signaling receptor activity was the top pathway, followed by various signaling and cell communication pathways.

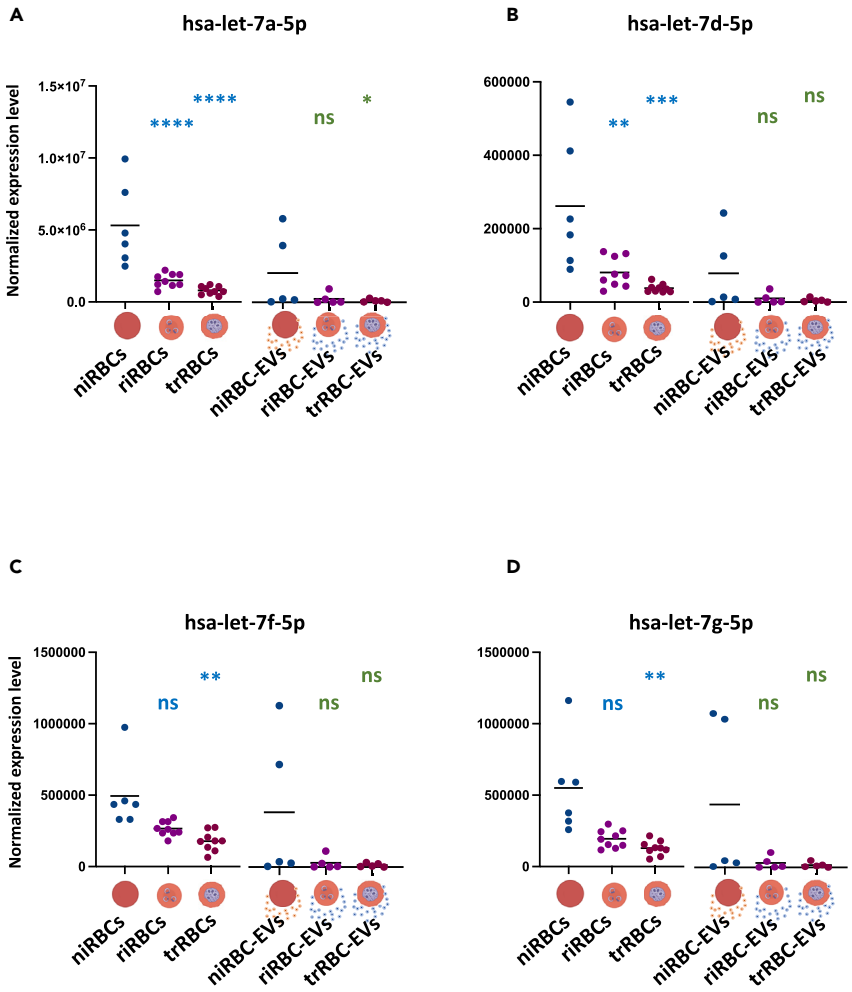

Figure 6. The expression levels of some hsa-let-7 family members in riRBCs and trRBCs versus niRBCs and in riRBC-EVs and trRBC-EVs versus niRBC-EVs

(A–D) (A) hsa-let-7a-5p, (B) hsa-let-7d-5p, (C) hsa-let-7f-5p and (D) hsa-let-7g-5p. The comparisons were done using the differential expression function in CLC Genomics software V22. Statistical significance was calculated using an FDR-adjusted p value <0.05 (ns = non-significant).

Differential expression of the let-7 family in iRBCs

Members of the let-7 family of miRNAs control cell signaling and immunomodulatory pathways. Figure 6 shows the expression profiles of some let-7 family members in niRBCs, iRBCs, and their EVs. The expression levels of let-7a-5p and let-7d-5p were downregulated significantly in both riRBCs and trRBCs versus niRBCs (Figures 6A and 6B). Within the EVs, hsa-let-7a-5p was only downregulated significantly in trRBC-EVs, and let-7d-5p expression was not affected significantly by *P. falciparum* infection. The expression levels of let-7f and let-7g were downregulated significantly in trRBCs (versus niRBCs), but their levels in the EVs were not affected significantly by *P. falciparum* infection (Figures 6C and 6D).

Differential expression of mRNAs in iRBCs versus niRBCs

Our findings from the miRNA analyses prompted us to examine whether the mRNA expression profile of human RBCs is also affected by *P. falciparum* infection. To this end, we performed NGS of mRNAs extracted from riRBCs, trRBCs, and niRBCs. The reads were aligned to the human transcriptome using the RNA-seq function of CLC Genomics software V22. FDR-adjusted p values were used to detect mRNAs that were differentially expressed in riRBCs and trRBCs versus niRBCs. Figure 7A shows a heatmap of the statistically significant differentially expressed genes. Overall, 20 and 30 mRNAs were significantly downregulated and upregulated, respectively, in the infected cells (Table S4). We calculated the

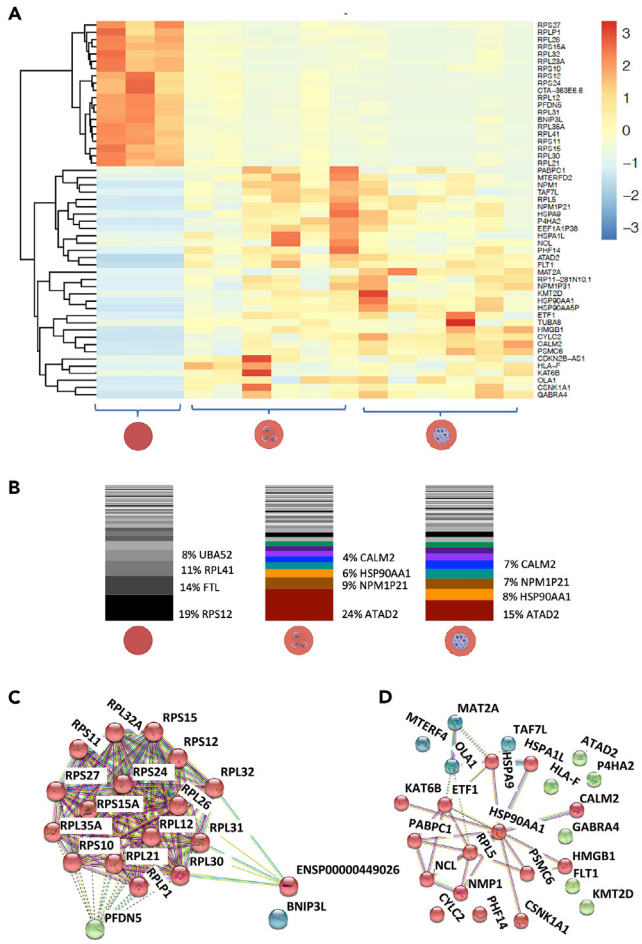

Figure 7. mRNA profiles of iRBCs compared to niRBCs

(A) A heatmap representing the expression levels of the most highly differentially expressed mRNAs in riRBCs and trRBCs versus niRBCs. The heatmap was produced using the pheatmap R package[38] (for the script, please see STAR Methods).

(B) A graphical presentation of the dominant transcripts within the cell populations described in (A).

(C and D) STRING clustering analyses of the proteins encoded by the genes that were downregulated (C) or upregulated (D) in iRBCs versus niRBCs. The blue and pink connector lines represent the database and experimentally confirmed interactions, respectively.

percentages of the dominant transcripts in niRBCs and found that riosomal protiens 12 (*RPS12*) and L ribosomal proteins 41 (*RPL41*) represented 19% and 11% of the total transcripts, respectively. These two genes encode cytoplasmic ribosomes. The expression levels of *RPS12* and *RPL41*, as well as other genes encoding cytoplasmic ribosomes, were downregulated significantly in RBCs after infection with *P. falciparum* (Figure 7B). In addition, riRBCs and trRBCs showed significant increases in the expression levels of the *ATAD2*, *CALM2*, and *HSP90α* mRNAs (Figure 7B). Figure 7C shows a K-means clustering analysis of the genes that were downregulated significantly in riRBCs and trRBCs versus niRBCs. These downregulated genes mainly encoded cytoplasmic ribosomal proteins (Figure 7D).

DISCUSSION

Genetic polymorphism that affects the host's response to pathogens might explain why 2% of malaria patients develop CM. Various cellular signals, including immune signaling pathways, require fine-tuned regulation during infection, and we postulate that these regulations occur, at least in part, via miRNAs. Indeed, there is substantial evidence to support the hypothesis that human miRNAs influence the outcome and complications of *P. falciparum* infection. miRNAs play a primary role in regulating gene expression by binding to target mRNAs and preventing their translation into proteins. Single miRNAs can bind to several genes involved in different pathways. In malaria, human miRNAs can penetrate *P. falciparum*-infected cells and form duplexes

with mRNAs, preventing their translation.[8] A previous study found that miR-150-5p was downregulated in whole blood from an adult infected with *P. falciparum*.[39] On the other hand, another study found that miR-150-5p was upregulated in plasma-derived EVs from patients infected with P. vivax.[40] C57BL76 mice infected with *P. berghei* asymmetric dimethylarginine-to-arginine (ANKA) develop CM and have higher expression levels of miR-27a and miR-142 in their brains than *P. yoelii*-infected mice without CM.[41] In addition, recent studies have identified miRNAs as crucial host factors that regulate parasite growth.[42,43]

miRNA profiles are tissue specific, and erythrocyte-derived miRNAs have been reported as potential biomarkers of specific diseases. A number of miRNAs that are up- or downregulated during erythropoiesis are selectively retained in mature RBCs.[5,21,44] Here, we characterized the effects of *P. falciparum* infection on the miRNA profiles of human RBCs and their secreted EVs. We found that miR-451a was the most abundant miRNA in both RBCs and RBC-EVs, an observation that is consistent with other studies. For example, miR-451a is reportedly abundant in cells of the erythroid lineage, including mature RBCs.[19] Chamnanchanunt and colleagues found that miR-451 was downregulated in plasma samples from patients with *P. vivax* infection.[40] Mantel et al. also demonstrated the internalization of iRBC-EVs within macrophages, where they initiate a strong inflammatory response.[45] Later, the same group found that miR-451a is present in iRBC-EVs and postulated that it is transported to ECs via these vesicles and subsequently alters their function.[28] This hypothesis contradicts our current finding that miR-451a levels in RBCs and RBC-EVs were the same before and after *P. falciparum* infection, suggesting that RBC-EVs deliver the same amount of miR-451a to recipient cells under uninfected and infected conditions. We speculate that the functional impairment of ECs in Mantel's experiments might have been due to other differentially expressed miRNAs that were transported within EVs, such as those identified in our current study.

In this study, we detected high expression of human miRNA candidates within *Plasmodium* iRBCs. In a study in 2012, LaMonte and colleagues reported the translocation of human miRNAs to *Plasmodium falciparum*,[8] suggesting that these miRNAs could be preserved from degradation within the parasite vacuole. However, our results do not support this possibility because we isolated miRNA from niRBCs and iRBCs at the same time, which gives no chance for miRNA degradation within the niRBCs. This was further confirmed by the results of experiments showing that miRNA profiles were not appreciably different in blood samples taken from different healthy individuals over a 2-year period.

Based on our experiments, we hypothesize that there might be minimal transcription happening within the RBCs even after enucleation. This is supported by other studies showing that RBCs contain RNA polymerase I, II, and III, as well as DNA-binding proteins (11). Also, RBCs express Toll-like receptor 9 (TLR9) on their surface, which scavenge cell-free CpG-DNA during quiescent states to prevent non-specific inflammation.[46,47] These small DNA fragments may act as templates for transcription. Further studies are needed to test this hypothesis.

In our study, we identified that nine miRNAs were significantly expressed at high levels in iRBCs and in their EVs at both the ring and trophozoite stages. To our knowledge, there have been no other reports of an association between these miRNAs and pathogenesis/severity of malaria. We attribute this shortfall to the fact that most studies isolate miRNAs from serum-derived EVs, which include EVs from different tissue origins.[48] *P. falciparum*-induced dysregulation of miRNAs could affect multiple cellular functions and pathological processes, depending on the target genes of the affected miRNAs. Our bioinformatic analysis uncovered several interesting targets of the infection-related differentially expressed miRNAs; hence, it would be useful to study the functions of these miRNAs and how they affect different recipient cells in more detail. The putative target genes identified here were clustered into four main groups, including cell signaling, HIF-1 and phagosome pathways, cytokine receptor activity, and immune-regulatory interactions. Accordingly, we plan to analyze the effects of these miRNAs and target genes in different recipient cells, such as ECs and other immune cells.

We found that miR-200a-3p, miR-200b-3p, and miR-200c-3p were upregulated in EVs isolated from both riRBCs and trRBCs (Tables S1 and S2). A previous study demonstrated that miR-200b and miR-200c mediate a proinflammatory response in patients with *Listeria* infection and that the expression levels of the protein-coding target genes are inversely correlated with those of the miRNAs.[49] Another study found that miR-200b and miR-200c play a role in neurodegenerative diseases by targeting genes that cause progressive degeneration of the structure of the central nervous system.[50] These results suggest that RBCs contribute to modulation of the immune response during *P. falciparum* infection; however, the mechanism underlying this process is currently unknown.

Several miRNAs in the let-7 family were downregulated significantly in both RBCs and RBC-EVs after *P. falciparum* infection (Tables S1 and S2). The let-7 family controls cell signaling pathways in many living organisms. Notably, let-7 reduces the potency of the innate immune response by repressing translation of the mRNA encoding Toll-like receptor 4 (TLR4), which controls the activation of nuclear factor κB and the expression of a set of downstream genes involved in inflammation. Downregulation of let-7 has also been reported in several viral diseases. Also, *Cryptosporidium parvum* infection was reported to be associated with reduced let-7i and increased TLR4 signaling. Let-7 also affects the differentiation of cluster of differentiation 8 (CD8)-positive T cells, which can release effector cytokines and eliminate infected target cells.[51–53]

In support of our finding that *P. falciparum* infection affects the miRNA profile of RBCs, alterations in host cell miRNA profiles have also been reported for other parasites.[54] For example, in *Leishmania donovani*¬-infected mice, the surface acid protease (gp63) of the parasite targets the host's Dicer1, cleaving Dicer to downregulate pre-miR-122 and its processing to miR-122, leading to reduced post-transcriptional regulation of its target mRNAs and increased pathogenicity.[55] In addition, miR-551 is reportedly upregulated in dendritic cells following *L. donovani* infection and can interfere with TLR4 signaling, which plays an important role in the activation of the antileishmanial immune response.[56] During *Toxoplasma gondii* infection, the expression of miR-17-92 is increased within infected cells, leading to inhibition of the proapoptotic molecule Bcl-2interactingmediator of cell death (BIM). This inhibition of apoptosis helps Toxoplasma evade the immune system.[57,58] Furthermore, in *Trypanosoma cruzi* infection, downregulation of miR-133 and miR-208 is correlated with the increased expression of cardiac genes that play a role in the cardiovascular complications seen in chronic Chagas disease patients.[59,60]

In early studies, technological limitations may have hampered the identification of low levels of mRNAs in RBCs.[61,62] In 2006, researchers detected small RNAs in RBCs for the first time.[63] This discovery was followed by the confirmation that RBCs express several different types of long RNAs (~8,092 genes).[9,10] The RBC transcriptome originates from the remaining transcriptome of differentiating erythroid cells that persists after enucleation and terminal differentiation. Previous studies have demonstrated that miRNAs target genes within RBCs, for example, miR-4732-3p, which targets Smad2 and Smad4.[19] Therefore, in addition to examining the miRNA profiles of niRBCs and iRBCs, we also characterized changes in the RBC mRNA profile after *P. falciparum* infection and found that the levels of the dominant transcripts in niRBCs (RPS12 and RPL41) were downregulated significantly after infection. We postulate that the residual translation of mRNAs in RBCs is regulated by miRNAs. However, we cannot exclude the possibility that some ribosomes in RBCs might be neglected due to the density of hemoglobin. A small number of ribosomes may be enough to complete translation, in which case, mature RBCs retain a few specific RNA species. We also performed an immunofluorescence analysis of niRBCs, riRBCs, and trRBCs using anti-DNA antibodies and identified tiny fragments of DNA (Figure S1). Further studies are required to validate these findings.

In summary, we examined the miRNA profiles of niRBCs and iRBCs, as well as their secreted EVs. The miRNA profiles of RBCs and their EVs were altered significantly after *P. falciparum* infection, and a bioinformatic prediction of the target genes suggested that several factors work together in a tightly regulated fashion to control the immune response during infection. Evidence from other studies suggests that RBC-miRNAs are transported inside EVs and taken up by various cells throughout the circulatory system, thereby affecting mRNA expression in these recipient cells. Further studies are required to clarify the functions of miRNAs in RBCs and RBC-EVs. Nonetheless, the results presented here contribute to current understanding of the dynamics of cell-cell communication during *P. falciparum* infection.

Limitations of the study

In this study, for more verification of the target mRNA prediction of the miRNA candidates, *in vitro* functional analysis should be conducted, but we plan this for our future studies.

STAR★METHODS

Detailed methods are provided in the online version of this paper and include the following:

- KEY RESOURCES TABLE
- RESOURCE AVAILABILITY
  - Lead contact
  - Materials availability

SUPPLEMENTAL INFORMATION

Supplemental information can be found online at https://doi.org/10.1016/j.isci.2023.107119.

ACKNOWLEDGMENTS

We would like to thank Prof. Egbert Tannich (BNITM) for substantial support at the beginning of the project and Heike Baum (BNITM) for support during NGS sequencing. Also, we thank Mohsin Shafiq (Institute for Neuropathology, Medical center Hamburg-Eppendorf-Germany) for help and support with Nanosight measurements. This work was supported by Chinese Scholarship Council (Yifan Wu), Jürgen Manchot Stiftung (Hanifeh Torabi), Joachim Herz Foundation (Barbara Honecker), and Leibniz Center Infection (Maria del Pilar Martinez Tauler).

AUTHOR CONTRIBUTIONS

Conceptualization, N.G.M.; methodology, Y.W., S.L., B.H., H.T., M.P.M.T., K.H., D.C., and N.G.M,; software, N.G.M.; validation, K.H., D.C., and N.G.M; formal analysis, N.G.M.; writing, original draft preparation, N.G.M; writing, review, and editing, Y.W., T.J., I.B., and N.G.M. All authors have read and agreed to the published version of the manuscript.

DECLARATION OF INTERESTS

The authors declare no competing interests.

INCLUSION AND DIVERSITY

One or more of the authors of this paper self-identifies as an underrepresented ethnic minority in their field of research or within their geographical location.

Received: November 21, 2022
Revised: March 8, 2023
Accepted: June 9, 2023
Published: June 15, 2023

REFERENCES

1. WHO (2021). WHO Malaria Report 2021 (WHO).

2. Rug, M., Prescott, S.W., Fernandez, K.M., Cooke, B.M., and Cowman, A.F. (2006). The role of KAHRP domains in knob formation and cytoadherence of P falciparum-infected human erythrocytes. Blood *108*, 370–378.

3. Kyes, S., Horrocks, P., and Newbold, C. (2001). Antigenic variation at the infected red cell surface in malaria. Annu. Rev. Microbiol. *55*, 673–707.

4. Newbold, C., Craig, A., Kyes, S., Rowe, A., Fernandez-Reyes, D., and Fagan, T. (1999). Cytoadherence, pathogenesis and the infected red cell surface in Plasmodium falciparum. Int. J. Parasitol. *29*, 927–937.

5. Chen, S.Y., Wang, Y., Telen, M.J., and Chi, J.T. (2008a). The genomic analysis of erythrocyte microRNA expression in sickle cell diseases. PLoS One *3*, e2360.

6. Kannan, M., and Atreya, C. (2010). Differential profiling of human red blood cells during storage for 52 selected microRNAs. Transfusion *50*, 1581–1588.

7. Sangokoya, C., Lamonte, G., and Chi, J.T. (2010). Isolation and characterization of microRNAs of human mature erythrocytes. Methods Mol. Biol. *667*, 193–203.

8. Lamonte, G., Philip, N., Reardon, J., Lacsina, J.R., Majoros, W., Chapman, L., Thornburg, C.D., Telen, M.J., Ohler, U., Nicchitta, C.V., et al. (2012). Translocation of sickle cell erythrocyte microRNAs into Plasmodium

falciparum inhibits parasite translation and contributes to malaria resistance. Cell Host Microbe *12*, 187–199.

9. Azzouzi, I., Moest, H., Wollscheid, B., Schmugge, M., Eekels, J.J.M., and Speer, O. (2015). Deep sequencing and proteomic analysis of the microRNA-induced silencing complex in human red blood cells. Exp. Hematol. *43*, 382–392.

10. Doss, J.F., Corcoran, D.L., Jima, D.D., Telen, M.J., Dave, S.S., and Chi, J.T. (2015). A comprehensive joint analysis of the long and short RNA transcriptomes of human erythrocytes. BMC Genomics *16*, 952.

11. Kabanova, S., Kleinbongard, P., Volkmer, J., Andrée, B., Kelm, M., and Jax, T.W. (2009). Gene expression analysis of human red blood cells. Int. J. Med. Sci. *6*, 156–159.

12. Bartel, D.P. (2009). MicroRNAs: target recognition and regulatory functions. Cell *136*, 215–233.

13. Khraiwesh, B., Arif, M.A., Seumel, G.I., Ossowski, S., Weigel, D., Reski, R., and Frank, W. (2010). Transcriptional control of gene expression by microRNAs. Cell *140*, 111–122.

14. Liang, Y., Ridzon, D., Wong, L., and Chen, C. (2007). Characterization of microRNA expression profiles in normal human tissues. BMC Genomics *8*, 166.

15. Zhou, M.H., Zhang, L., Song, M.J., and Sun, W.J. (2018). MicroRNA-218 prevents lung injury in sepsis by inhibiting RUNX2. Eur. Rev. Med. Pharmacol. Sci. *22*, 8438–8446.

16. Chakraborty, C., Sharma, A.R., Sharma, G., Doss, C.G.P., and Lee, S.S. (2017). Therapeutic miRNA and siRNA: Moving from Bench to Clinic as Next Generation Medicine. Mol. Ther. Nucleic Acids *8*, 132–143.

17. Ruiz-Tagle, C., Naves, R., and Balcells, M.E. (2020). Unraveling the Role of MicroRNAs in Mycobacterium tuberculosis Infection and Disease: Advances and Pitfalls. Infect. Immun. *88*, e00649-19.

18. Sun, L., Yu, Y., Niu, B., and Wang, D. (2020). Red Blood Cells as Potential Repositories of MicroRNAs in the Circulatory System. Front. Genet. *11*, 442. https://doi.org/10.3389/fgene.2020.00442.

19. Chen, Y., Liu, W., Chao, T., Zhang, Y., Yan, X., Gong, Y., Qiang, B., Yuan, J., Sun, M., and Peng, X. (2008b). MicroRNA-21 down-regulates the expression of tumor suppressor PDCD4 in human glioblastoma cell T98G. Cancer Lett. *272*, 197–205.

20. Juzenas, S., Venkatesh, G., Hübenthal, M., Hoeppner, M.P., Du, Z.G., Paulsen, M., Rosenstiel, P., Senger, P., Hofmann-Apitius, M., Keller, A., et al. (2017). A comprehensive, cell specific microRNA catalogue of human peripheral blood. Nucleic Acids Res. *45*, 9290–9301.

21. Ryan, P., and Atreya, C. (2011). Blood cell microRNAs: what are they and what future do they hold? Transfus. Med. Rev. *25*, 247–251. https://doi.org/10.1016/j.tmrv.2011.01.005.

22. Teruel-Montoya, R., Kong, X., Abraham, S., Ma, L., Kunapuli, S.P., Holinstat, M., Shaw, C.A., Mckenzie, S.E., Edelstein, L.C., and Bray, P.F. (2014). MicroRNA expression differences in human hematopoietic cell lineages enable regulated transgene expression. PLoS One *9*, e102259.

23. Li, K.Y., Zheng, L., Wang, Q., and Hu, Y.W. (2016). Characteristics of erythrocyte-derived microvesicles and its relation with atherosclerosis. Atherosclerosis *255*, 140–144.

24. Chakrabarti, M., Garg, S., Rajagopal, A., Pati, S., and Singh, S. (2020). Targeted repression of Plasmodium apicortin by host microRNA impairs malaria parasite growth and invasion. Dis Model Mech *13*, dmm042820. https://doi.org/10.1242/dmm.042820.

25. Dandewad, V., Vindu, A., Joseph, J., and Seshadri, V. (2019). Import of human miRNA-RISC complex into Plasmodium falciparum and regulation of the parasite gene expression. J. Biosci. *44*, 50.

26. Arroyo, J.D., Chevillet, J.R., Kroh, E.M., Ruf, I.K., Pritchard, C.C., Gibson, D.F., Mitchell, P.S., Bennett, C.F., Pogosova-Agadjanyan, E.L., Stirewalt, D.L., et al. (2011). Argonaute2 complexes carry a population of circulating microRNAs independent of vesicles in human plasma. Proc. Natl. Acad. Sci. USA *108*, 5003–5008.

27. Mantel, P.Y., Hjelmqvist, D., Walch, M., Kharoubi-Hess, S., Nilsson, S., Ravel, D., Ribeiro, M., Grüring, C., Ma, S., Padmanabhan, P., et al. (2016). Infected erythrocyte-derived extracellular vesicles alter vascular function via regulatory Ago2-miRNA complexes in malaria. Nat. Commun. *7*, 12727.

28. Mantel, P.Y., and Marti, M. (2014). The role of extracellular vesicles in Plasmodium and other protozoan parasites. Cell Microbiol. *16*, 344–354.

29. Willeit, P., Zampetaki, A., Dudek, K., Kaudewitz, D., King, A., Kirkby, N.S., Crosby-Nwaobi, R., Prokopi, M., Drozdov, I., Langley, S.R., et al. (2013). Circulating microRNAs as novel biomarkers for platelet activation. Circ. Res. *112*, 595–600.

30. Zhang, Y., Roccaro, A.M., Rombaoa, C., Flores, L., Obad, S., Fernandes, S.M., Sacco, A., Liu, Y., Ngo, H., Quang, P., et al. (2012). LNA-mediated anti-miR-155 silencing in low-grade B-cell lymphomas. Blood *120*, 1678–1686. https://doi.org/10.1182/blood-2012-04-425207.

31. Vu, L., Ragupathy, V., Kulkarni, S., and Atreya, C. (2017). Analysis of Argonaute 2-microRNA complexes in ex vivo stored red blood cells. Transfusion *57*, 2995–3000. https://doi.org/10.1111/trf.14325.

32. Trager, W., and Jensen, J.B. (2005). Human malaria parasites in continuous culture. 1976. J. Parasitol. *91*, 484–486.

33. Lambros, C., and Vanderberg, J.P. (1979). Synchronization of Plasmodium falciparum erythrocytic stages in culture. J. Parasitol. *65*, 418–420.

34. Pisitkun, T., Shen, R.F., and Knepper, M.A. (2004). Identification and proteomic profiling of exosomes in human urine. Proc. Natl. Acad. Sci. USA *101*, 13368–13373.

35. Szatanek, R., Baj-Krzyworzeka, M., Zimoch, J., Lekka, M., Siedlar, M., and Baran, J. (2017). The Methods of Choice for Extracellular Vesicles (EVs) Characterization. Int. J. Mol. Sci. *18*, 1153.

36. Wu, C.W., Cao, X., Berger, C.K., Foote, P.H., Mahoney, D.W., Simonson, J.A., Anderson, B.W., Yab, T.C., Taylor, W.R., Boardman, L.A., et al. (2017). Novel Approach to Fecal Occult Blood Testing by Assay of Erythrocyte-Specific microRNA Markers. Dig. Dis. Sci. *62*, 1985–1994.

37. R Core Team (2022). R: A Language and Environment for Statistical Computing (R Foundation for Statistical Computing). https://www.R-project.org/.

38. Kolde, R. (2012). Pheatmap: Pretty Heatmaps (R Package Version).

39. Kaur, H., Sehgal, R., Kumar, A., Sehgal, A., Bansal, D., and Sultan, A.A. (2018). Screening and identification of potential novel biomarker for diagnosis of complicated *Plasmodium vivax*malaria. J. Transl. Med. *16*, 272.

40. Chamnanchanunt, S., Kuroki, C., Desakorn, V., Enomoto, M., Thanachartwet, V., Sahassananda, D., Sattabongkot, J., Jenwithisuk, R., Fucharoen, S., Svasti, S., and Umemura, T. (2015). Downregulation of plasma miR-451 and miR-16 in Plasmodium vivax infection. Exp. Parasitol. *155*, 19–25. https://doi.org/10.1016/j.exppara.2015.04.013.

41. Martin-Alonso, A., Cohen, A., Quispe-Ricalde, M.A., Foronda, P., Benito, A., Berzosa, P., Valladares, B., and Grau, G.E. (2018). Differentially expressed microRNAs in experimental cerebral malaria and their involvement in endocytosis, adherens junctions, FoxO and TGF-β signalling pathways. Sci. Rep. *8*, 11277. https://doi.org/10.1038/s41598-018-29721-y.

42. Chang, T.-C., and Mendell, J.T. (2007). microRNAs in vertebrate physiology and human disease. Annu. Rev. Genomics Hum. Genet. *8*, 215–239. https://doi.org/10.1146/annurev.genom.8.080706.092351.

43. Rubio, M., Bassat, Q., Estivill, X., and Mayor, A. (2016). Tying malaria and microRNAs: from the biology to future diagnostic perspectives. Malar. J. *15*, 167. https://doi.org/10.1186/s12936-016-1222-9.

44. Hamilton, A.J. (2010). MicroRNA in erythrocytes. Biochem. Soc. Trans. *38*, 229–231. https://doi.org/10.1042/BST0380229.

45. Mantel, P.Y., Hoang, A.N., Goldowitz, I., Potashnikova, D., Hamza, B., Vorobjev, I., Ghiran, I., Toner, M., Irimia, D., Ivanov, A.R., et al. (2013). Malaria-infected erythrocyte-derived microvesicles mediate cellular communication within the parasite population and with the host immune system.

Cell Host Microbe *13*, 521–534. https://doi.org/10.1016/j.chom.2013.04.009.

46. Lam, L.K.M., Murphy, S., Kokkinaki, D., Venosa, A., Sherrill-Mix, S., Casu, C., Rivella, S., Weiner, A., Park, J., Shin, S., et al. (2021). DNA binding to TLR9 expressed by red blood cells promotes innate immune activation and anemia. Sci. Transl. Med. *13*, eabj1008. https://doi.org/10.1126/scitranslmed.abj1008.

47. Hotz, M.J., Qing, D., Shashaty, M.G.S., Zhang, P., Faust, H., Sondheimer, N., Rivella, S., Worthen, G.S., and Mangalmurti, N.S. (2018). Red Blood Cells Homeostatically Bind Mitochondrial DNA through TLR9 to Maintain Quiescence and to Prevent Lung Injury. Am. J. Respir. Crit. Care Med. *197*, 470–480. https://doi.org/10.1164/rccm.201706-1161OC.

48. Ketprasit, N., Cheng, I.S., Deutsch, F., Tran, N., Imwong, M., Combes, V., and Palasuwan, D. (2020). The characterization of extracellular vesicles-derived microRNAs in Thai malaria patients. Malar. J. *19*, 285. https://doi.org/10.1186/s12936-020-03360-z.

49. Izar, B., Mannala, G.K., Mraheil, M.A., Chakraborty, T., and Hain, T. (2012). microRNA response to Listeria monocytogenes infection in epithelial cells. Int. J. Mol. Sci. *13*, 1173–1185.

50. Sundararajan, V., Burk, U.C., and Bajdak-Rusinek, K. (2022). Revisiting the miR-200 Family: A Clan of Five Siblings with Essential Roles in Development and Disease. Biomolecules *12*, 781.

51. Chen, X.M., Splinter, P.L., O'hara, S.P., and Larusso, N.F. (2007). A cellular micro-RNA, let-7i, regulates Toll-like receptor 4 expression and contributes to cholangiocyte immune responses against Cryptosporidium parvum infection. J. Biol. Chem. *282*, 28929–28938.

52. Kumar, M., Sahu, S.K., Kumar, R., Subuddhi, A., Maji, R.K., Jana, K., Gupta, P., Raffetseder, J., Lerm, M., Ghosh, Z., et al. (2015). MicroRNA let-7 modulates the immune response to Mycobacterium tuberculosis infection via control of A20, an inhibitor of the NF-kappaB pathway. Cell Host Microbe *17*, 345–356.

53. Wells, A.C., Daniels, K.A., Angelou, C.C., Fagerberg, E., Burnside, A.S., Markstein, M., Alfandari, D., Welsh, R.M., Pobezinskaya, E.L., and POBEZINSKY, L.A. (2017). Modulation of let-7 miRNAs controls the differentiation of effector CD8 T cells. Elife *6*, e26398.

54. Acuña, S.M., Floeter-Winter, L.M., and Muxel, S.M. (2020). MicroRNAs: Biological Regulators in Pathogen-Host Interactions. Cells *9*, 113. https://doi.org/10.3390/cells9010113.

55. Ghosh, J., Bose, M., Roy, S., and Bhattacharyya, S.N. (2013). Leishmania donovani targets Dicer1 to downregulate miR-122, lower serum cholesterol, and facilitate murine liver infection. Cell Host Microbe *13*, 277–288. https://doi.org/10.1016/j.chom.2013.02.005.

56. Tolouei, S., Hejazi, S.H., Ghaedi, K., Khamesipour, A., and Hasheminia, S.J. (2013). TLR2 and TLR4 in cutaneous leishmaniasis caused by Leishmania major. Scand. J. Immunol. *78*, 478–484. https://doi.org/10.1111/sji.12105.

57. Goebel, S., Gross, U., and Lüder, C.G. (2001). Inhibition of host cell apoptosis by Toxoplasma gondii is accompanied by reduced activation of the caspase cascade and alterations of poly(ADP-ribose) polymerase expression. J. Cell Sci. *114*, 3495–3505. https://doi.org/10.1242/jcs.114.19.3495.

58. O'Connor, L., Strasser, A., O'Reilly, L.A., Hausmann, G., Adams, J.M., Cory, S., and Huang, D.C. (1998). Bim: a novel member of the Bcl-2 family that promotes apoptosis. EMBO J. *17*, 384–395. https://doi.org/10.1093/emboj/17.2.384.

59. Abel, L.C., Rizzo, L.V., Ianni, B., Albuquerque, F., Bacal, F., Carrara, D., Bocchi, E.A., Teixeira, H.C., Mady, C., Kalil, J., and Cunha-Neto, E. (2001). Chronic Chagas' disease cardiomyopathy patients display an increased IFN-gamma response to Trypanosoma cruzi infection. J. Autoimmun. *17*, 99–107. https://doi.org/10.1006/jaut.2001.0523.

60. Nogueira, L.G., Santos, R.H.B., Ianni, B.M., Fiorelli, A.I., Mairena, E.C., Benvenuti, L.A., Frade, A., Donadi, E., Dias, F., Saba, B., and Cunha-Neto, E. (2012). Myocardial chemokine expression and intensity of myocarditis in Chagas cardiomyopathy are controlled by polymorphisms in CXCL9 and CXCL10. PLoS Negl. Trop. Dis. *6*, e1867.

61. Lee, L.G., Chen, C.H., and Chiu, L.A. (1986). Thiazole orange: a new dye for reticulocyte analysis. Cytometry *7*, 508–517. https://doi.org/10.1002/cyto.990070603.

62. Rathjen, T., Nicol, C., McConkey, G., and Dalmay, T. (2006). Analysis of short RNAs in the malaria parasite and its red blood cell host. FEBS Lett. *580*, 5185–5188. https://doi.org/10.1016/j.febslet.2006.08.063.

63. Rainen, L., Oelmueller, U., Jurgensen, S., Wyrich, R., Ballas, C., Schram, J., Herdman, C., Bankaitis-Davis, D., Nicholls, N., Trollinger, D., and Tryon, V. (2002). Stabilization of mRNA expression in whole blood samples. Clin. Chem. *48*, 1883–1890.

64. Fu, Y., Wu, P.H., Beane, T., Zamore, P.D., and Weng, Z. (2018). Elimination of PCR duplicates in RNAseq and small RNA-seq using unique molecular identifiers. BMC Genomics *19*, 531.

STAR★METHODS

KEY RESOURCES TABLE

REAGENT or RESOURCE	SOURCE	IDENTIFIER
Antibodies		
α human CD235a -HI264	Biolegend, San Diego, USA	Cat#349103
goat-anti mouse colloidal gold-conjugated secondary antibody	Jackson Immuno Research, Cambridge shire, UK	–
CALM2 monoclonal antibody	MyBiosource.com	Cat#MBS200093
Anti-HSP90α	Merck	Cat#CA1023-50UG
ALEXA FLUOR 488	Thermo Fisher Scientific	Cat#A28175
Biological samples		
Human red blood cells (RBCs)	University Clinic-Eppedorf-Hamburg-Germany	Human Blood (0+)
Human Serum	Interstate Blood Bank, Inc (Memphis, USA).	A+
Chemicals, peptides, and recombinant proteins		
RPMI 1640	Applichem	Cat#A1538,9010
Hypoxanthine	Sigma	Cat#H9636-56
Gelatin from porcine skin-175 g bloom type A	Sigma	Cat#G2625
D-Sorbitol	Sigma	Cat#S1876
Critical commercial assays		
QUbit ™ Protein Assay Kit	ThermoFisher Scientific, Waltham, USA	Cat#Q33211
Ultrafiltration units 100,000 MWCO PES	Sartorius, Göttingen, Germany	Cat#VS2042
miRNeasy mini-Kit	Qiagen, Hilden, Germany	Cat#5067-1513
Agilent 2100® bioanalyzer Pico-Kit	Agilent	
QIAseq Standard mRNA Select Kit (96)	Qiagen	Cat#180775
NextSeq 500/550 Mid Output Kit v.25 (150 Cycles)	illumina	Cat#20024904
QuDye dsDNA HS Assay Kit	Lumiprobe	Cat#12102
Deposited data		
Bioproject	NCBI	Number: PRJNA897869
Software and algorithms		
NanoSight Software	–	(NTA3 0064)
Agilent 2100® bioanalyzer software	Santa Clara, USA	
CLC genomics work bench	Qiagen, Aarhus	version 21
IPA	Qiagen, Aarhus	–
Graphpad Prism	San Diego, California	Version 9.4.1

RESOURCE AVAILABILITY

Lead contact

Further information and requests for resources should be directed to the lead contact, Nahla Galal Metwally metwally@bnitm.de.

Materials availability

This study did not generate new unique reagents.

Data and code availability

The RNA-sequencing data has been deposited at the NCBI and is publically available as of the date of publication.

The bioproject Number is PRJNA897869. All other original data reported in this paper will be shared by the lead contact upon request. This paper does not report original code.

Any additional information required to reanalyse the data reported in this paper is available from the lead contact upon request.

EXPERIMENTAL MODEL AND SUBJECT DETAILS

In these experiments we used IT4- *P. falciparum* iRBCs to characterize RBC-miRNAs, RBC-EV-miRNAs, and RBC-mRNAs. niRBCs and IT4- *P. falciparum* iRBCs were cultivated in RPMI medium with human serum.[32] Synchronisation for the *P. falciparum* culture was performed using sorbitol.[33] RBC-miRNAs and RBC-mRNAs were isolated from RBCs as controls. The RBC-EVs purification was performed from the culture supernatants of niRBCs, riRBCs, and trRBCs, as described (see below).[28] Subsequently, RBC-EV-miRNAs were isolated. The RBC-miRNAs, RBC-EV-miRNAs, and RBC-mRNAs were then sequenced and the obtained sequences were aligned to the human miRNA/transcriptome reference sequences.

METHOD DETAILS

P. falciparum culture

The IT4 (FCR3S1.2) isolate was cultivated in RPMI medium in the presence of 10% human serum A+ (Interstate Blood Bank, Inc. Memphis, TN, USA) and human O+ erythrocytes (5% hematocrit; UKE, Hamburg, Germany) according to standard procedures.[32] Parasite cultures were synchronized once per week using 5% sorbitol.[33] Trophozoites were enriched using 1% gelatine solution on the day of harvest to remove niRBCs. Then, the 80–90% trRBCs were lysed in 4X Trizol and stored at −80°C until the miRNA/mRNA purification step. Part of the enriched trRBC sample was cultivated with sufficient medium and niRBCs to allow approximately 70–90% riRBCs to be reached on the day after initiating cultivation. The riRBCs were lysed in 4X Trizol and kept at −80°C until the miRNA/mRNA purification step. niRBCs were also incubated in vesicle-free medium for two days before miRNA/mRNA purification as a control.

Extracellular vesicles purification

iRBCs-EVs were isolated from IT4 *P. falciparum* cell culture with 10% parasitemia as previously described.[27] In brief, the medium was changed to vesicle-depleted RPMI medium (depletion was done by centrifugation at 100,000 rcf for 90 min at 4°C). On the next day, (28 h after changing the medium), the cell culture supernatants (100 mL from 10 Petri dishes) were collected and sequentially centrifuged at 600 g, 1600 g, 3600 g and 10,000 g for 15 min each. After each step, the respective supernatant was collected for the next centrifugation step. To concentrate the EVs, the suspension was passed through ultrafiltration units (100,000 MWCO PES; Sartorius, Göttingen, Germany) for 30 min at 3000 g. The EVs contained in the concentrated supernatant were dissolved in PBS, layered on top of a 60% sucrose cushion, and centrifuged at 100,000 g for 16 h at 4°C. The interphase was collected and washed with PBS twice at 100,000 g for 60 min at 4°C. EVs were resuspended and pooled in 1000 µL PBS (0.2 µm filtered) and stored in 200 µL aliquots at −80°C. For isolation of EVs from uninfected RBCs (RBC-EV), which were used as negative controls in subsequent experiments, 10 petri dishes of 500 µL human blood 0+ (UKE Hamburg, Germany) and 10 mL *P. falciparum* culture medium for EV isolation were incubated at 37°C. After 28 h supernatants were collected and processed as described above. Protein concentration of EV samples was determined using the QUBIT Protein Assay Kit (ThermoFisher Scientific, Waltham, USA) according to manufacturer's instructions and by measuring the A_{280} content on a Nanodrop2000 (ThermoFisher Scientific, Waltham, USA).

Electron microscopy

Glow-discharged carbon- and formvar-coated nickel grids (Plano GmbH, Wetzlar, Germany) were incubated with aliquots of freshly isolated EVs. After washing with PBS and incubation in the blocking buffer (0.5% BSA in PBS), the EVs on the grids were labeled with the primary antibody (α human CD235a -HI264, Biolegend, San Diego, USA) at a concentration of 1:100 v/v in PBS (PAA-Laboratories GmbH, Pasching, Austria) containing 0.5% BSA (Sigma-Aldrich, Steinheim, Germany) for at least 21 h at 4°C. The controls for antibody specificity included omitting the primary antibody from the incubating solution. After the

incubation period, the grids were rinsed in buffer and further incubated with a goat-anti mouse colloidal gold-conjugated secondary antibody (12 nm gold particles from Jackson Immuno Research, Cambridgeshire, UK) at a dilution of 1:100 v/v for at least 21 h at 4°C. Nickel grids were rinsed in buffer and stained with 2% aqueous uranyl acetate (Electron Microscopy Sciences, Hatfield, USA) for 15 s. Grids were finally observed under a Tecnai Spirit electron microscope (Thermo Fisher Scientific, Waltham, USA) operating at 80 kV, and images were recorded with a digital CCD camera.

Nano particle tracking analysis (NTA) with Nanosight NS300

Purified EVs pellet were diluted 1:300 in PBS. The following settings were set according to the manufacturer's software manual (NanoSight LM10 User Manual, MAN0510-04-EN, 2015): the camera level was increased until all particles were distinctly visible (level16 and gain=20). A total number of 900 frames was recorded in each session (camera: CCD). The autofocus was adjusted to avoid indistinct particles. For each measurement, five 1-min videos were captured under the following conditions: cell temperature: 25°C; Frame rate/FBS: 30. After capture, the videos were analyzed by the in-build NanoSight Software (NTA3 0064) with a detection threshold of 6 and screen gain of 10.

Immunofluorescence assays

Blood smears (10 μL) were taken from IT4 *P. falciparum* cultures with 1–3% parasitaemia. The smears were fixed in acetone for 30 min and then rehydrated with 1x PBS for 5 min. The first antibody (1:20 in 3% BSA/PBS; CALM2 monoclonal antibody #MBS200093 (MyBiosource.com) or anti-HSP90α #CA1023-50UG (Merck) was then added and the slides were incubated for one hour in a humid dark box. The smears were washed 5x with 1X PBS and then labelled with AlexaFluor (1:1000) (Thermo Fisher # A28175) and DAPI (1mg/mL) (1:1000) (Roche # 10236276001) for 1 h in a humid dark box. After a 5x wash with 50 μL 1x PBS, the smears were air dried and Moviol was added before they were covered with a plastic cover slip. Images were taken through a EVOS FL auto-inverted microscope (Thermo Fisher Scientific, Waltham, USA) and analysed using ImageJ 1.53K. To calculate the corrected total cell fluorescence (CTCF), the following formula was used: Integrated Density – (Area of selected cell X Mean fluorescence of background readings).

mRNA purification and sequencing

Samples in Trizol were thawed before adding 200 μL chloroform and centrifugation for 30 min at 4°C and 12000 rpm. The miRNeasy mini-Kit- (Qiagen, Hilden, Germany) was used according to the manufacturer's instructions. The quality of mRNA/miRNA was assessed using the Agilent 2100® bioanalyzer system. According to the manufacturer's instructions, Ribosomal RNA was removed using QIAseq FastSelect RNA Removal Kit. The QIAseq Stranded mRNA Select Kit was used for mRNA enrichment. mRNA was sequenced using NextSeq 500/550 Mid Output Kit v2.5 (150 Cycles).

miRNA purification and sequencing

Samples in Trizol were thawed before adding 140 μL chloroform and centrifugation for 15 min at 4°C and 12000 rpm. The miRNeasy mini-Kit- (Qiagen, Hilden, Germany) was used according to the manufacturer's instructions. The quality of mRNA/miRNA was assessed using the Agilent 2100® bioanalyzer system. miRNA library preparation was performed in BGI Genomics – China. The small RNAs (18–30 nt) were purified by PAGE. For adapter ligation, the purified RNA was incubated with 3′ adapter followed by the 5′ adapter. Reverse transcription PCR was then performed and the PCR product was purified by PAGE. After denaturating and circularizing the DNA product, single-stranded circular DNA molecules were replicated via rolling cycle amplification, and a DNA nanoball (DNB) containing multiple copies of DNA was generated. DNBseq-UMI was then performed and about 18 M reads were generated per sample. UMI is known to correct the quantitative bias caused by PCR amplification of more than 70% small RNAs.[64]

Data analysis

Bioinformatics analysis was conducted using CLC genomics work bench version 22 (Qiagen, Aarhus). Clean reads were imported, and miRNA was quantified and annotated on the miRbase v22. Differential expression was performed, and P-values were adjusted using FDR 10%. hsg19 was used as a mRNA reference.

CLC Parameters (miRNA-Quantification)

miRBase: miRBase-Release_v22 / Prioritized species = Homo sapiens / Allow length based isomiRs = Yes / Additional upstream bases = 2 / Maximum mismatches = 2 / Strand specific = Yes / Minimum sequence length = 18 / Maximum sequence length = 25.

CLC differential expression Parameters (miRNA/mRNA)

Whole transcriptome RNA-seq / Normalization Method = TMM / Filter on Average expression for FDR correction / Result Handling = Save.

CLC Trim Parameters(mRNA)

Trim using quality scores = Yes / Quality limit = 0.05 / Trim ambiguous nucleotides = Yes / Maximum number of ambiguities = 2 / Automatic read-through adapter trimming = Yes / Remove 5′ terminal nucleotides = No / Remove 3′ terminal nucleotides = No / Trim to a fixed length = No / Maximum length = 150 / Trim end = Trim from 3′-end / Discard short reads = No / Discard long reads = No / Save discarded sequences = No / Save broken pairs = No / Create report = Yes.

CLC RNA-seq Parameters (mRNA)

Enable spike-ins = No / Database files = Homo sapiens (hg19) sequence / Maximum cost = 2 / Similarity fraction = 0.8 / Auto-detect paired distances = Yes / Maximum number of hits for a read = 10 / Strand setting = Both / Minimum supporting count = 5 / Create report = Yes / Unmapped reads = No / Expression value = Total count.

ADDITIONAL RESOURCES

R script for volcano plot generation

```
library("xlsx")

library ("ggplot2")

library ("purrr")

library ("tibble")

library ("dplyr")

library ("tidyr")

library ("stringr")

library ("readr")

library ("forcats")

D <- read.xlsx("00.xlsx", 1)

head(D)

# Make a basic volcano plot

with(D, plot(Rings.FC,-log2(R..P.value), pch=16, main="b", xlim=c(-30,30), ylim=c(0,25)))

with(subset(D, Rings.FC>5 ), points(Rings.FC, -log2(R..P.value), pch=16, col="tomato1"))

with(subset(D, Rings.FC< -5 ), points(Rings.FC, -log2(R..P.value), pch=16, col="olivedrab3"))
```

R script for volcano plot generation

```
library(pheatmap)
```

```
library(RColorBrewer)

library(ggplot2)

library("xlsx")

D <- read.xlsx("mirrbcs.xlsx", 1)

head(D)

row.names(D) <- D$Name

D1=subset(D,select=-Name) #remove row names

D_matrix <- data.matrix(D1)

D_heatmap <- pheatmap(D_matrix, color = colorRampPalette
  ((brewer.pal(n = 1, name ="RdYlBu")))(1000),
  margin=c(8,6),
  cellwidth = 20, cellheight = 5, scale="row",
  main = "",
  notecol="black", breaks = NA, cutree_cols = 1000,
  border_color = NA, fontsize_col = 5, fontsize_row = 5,
  kmeans_k = NA, cluster_rows=FALSE, cluster_cols=FALSE,
  angle_col = "45",
  treeheight_col = 1000, height = 10000, show_colnames =T,
  show_rownames = T).
```